Electrochemical and Computational Studies on the Corrosion Inhibition of Mild Steel by 1-Hexadecyl-3-methylimidazolium Bromide in HCl Medium

Jianhong Tan[1], Lei Guo[2,*], Dan Wu[1], Shanfei Wang[1], *Rongrong Yu[2], Fan Zhang[3], Savaş Kaya[4]*

[1] School of Chemistry and Chemical Engineering, Yangtze Normal University, Chongqing 408100, China
[2] School of Material and Chemical Engieering, Tongren University, Tongren 554300, China
[3] Division of Surface and Corrosion Science, Department of Chemistry, KTH Royal Institute of Technology, Stockholm SE-10044, Sweden
[4] Cumhuriyet University, Faculty of Science, Department of Chemistry, 58140, Sivas, Turkey
[*]E-mail: cqglei@163.com

An imidazolium-based ionic liquid, *i.e.*, 1-Hexadecyl-3-methylimidazolium Bromide (HMIBr), was investigated as a corrosion inhibitor candidate for mild steel in 1 M HCl medium using combined electrochemical and molecular simulation methods. Potentiodynamic polarization results show that HMIBr is a mixed-type inhibitor and suppresses the corrosion process effectively at optimum concentration 10^{-3} M with 96.9% inhibition efficiency. Electrochemical impedance spectroscopy (EIS) analysis indicated an increase in the charge transfer resistance with enhance of inhibitor concentration, and confirmed the adsorption of HMIBr on the iron surface. Moreover, density functional theory (DFT) calculations, Monte Carlo as well as molecular dynamics simulations were employed to obtain further insights into the antiseptic mechanism. Our findings have important guiding significance for understanding the corrosion inhibition mechanism and designing new ionic liquid-based inhibitor molecules.

1. INTRODUCTION

Steel materials have always played a very important role in the industrial field for many years. But unfortunately, steel is often subject to severe corrosion in the service environment, which has caused huge economic losses and environmental damage. Statistically, the costs of corrosion in most countries generally occupied approximately 2~5% of the national GNP [1]. Nowadays, lots of anti-corrosion approaches have been developed, such as coating, anode (cathode) protection, alloying, corrosion

inhibitor, surface treatments, metal plating, etc. Most people think that using corrosion inhibitors is a relatively convenient and efficient way for protecting metals, especially in the field of pickling [2, 3]. The common acid inhibitors are organic molecules containing heteroatoms (N, S, O, P), polar functional groups, π-electrons as well as aromatic rings in their structures [4]. Generally the suppression efficiency of the homologous series of corrosion inhibitors differing only in the heteroatoms follows the order: P > S > N > O [5]. Nevertheless, the actual inhibition performance is related to some other factors, such as molecular volume, solution temperature/pH, inhibitor concentration, etc. The inhibiting mechanism is generally interpreted by the formation of a physical and/or chemical adsorption barrier on the metal surface [6]. Although a spectrum of spectroscopy methods (such as XPS, SEM, FT-IR) have been shown to be effective in explaining the corrosion inhibition mechanism over the last few decades, directly imaging inhibitor molecules residing in the metal surafce has long been a challenge. Fortunately, with the development of computer technology and the constant enhancement of the ability to deal with data, the recognition of adsorption configurations for the inhibitor/metal systems can be implemented by molecular simulation [7].

In recent years, ionic liquids, which consist of organic cations and anions, are receiving much attention owing to their unique properties such as excellent thermal stability, high ionic conductivity, negligible vapor pressure, large electrochemical windows and lower-toxicity. As far as we know, some imidazolium-based ionic liquids have been proved to be effective corrosion inhibitors for carbon steels in acid medium [8-10]. Their inhibition performance is very susceptible to the alkyl chain length as well as the type of the anions.

In this account, another ionic liquid, HMIBr, was used as a potential inhibitor for mild steel corrosion in 1 M HCl solution. Techniques applied include the electrochemical measurements, DFT calculations, Monte Carlo (MC) as well as molecular dynamics (MD) simulations. Our work can push forward the progress on versatile ionic liquids with multifunctional abilities in the application of pickling industry.

2. EXPERIMENTAL

2.1. Materials and chemicals

Mild steel bar (composition: 0.15% C, 0.03% Mn, 0.02% Cr, 0.12% Si, 0.18% Al, and balance Fe) was cut mechanically into 2.5 cm × 2.0 cm × 0.30 cm^3 specimens and used as working electrodes. The contact area between the electrode surface and the corrosive medium was 1 cm^2. Prior to each test, the iron electrode sample was successively abraded with SiC emery papers of different grades (200, 400, 600, 800, and 1000), washed with running tap water followed by distilled water, immersed in ethanol and placed in a desiccator for use. HMIBr (≥99%) was purchased from Sigma-Aldrich and used devoid of any extra sanitization. The corrosive solution was prepared by dilution of analytical grade 37% HCl with doubly distilled water. The concentration effect of HMIBr towards the iron corrosion rate was examined at 1×10^{-5}, 5×10^{-5}, 2×10^{-4}, and 1×10^{-3} M.

2.2. Electrochemical experiments

The electrochemical measurements were conducted by a common three-electrode system operating on the RST5000 electrochemical analyzer. A saturated calomel electrode (SCE) and a platinum foil electrode were treated as reference and counter electrodes, respectively. Firstly, the iron electrode was immersed into the HCl solution for 1.5 h in order to attain a steady-state potential. After that, EIS test was performed at the open circuit potential (E_{ocp}), applying a sine wave with 10 mV amplitude in the frequency range of 100 kHz to 100 mHz. The obtained EIS data were analyzed through the ZsimpWin software. Finally, potentiodynamic polarization measurement was recorded by changing the electrode potential manually from −250 to +250 mV at E_{ocp} with a scan rate of 0.2 mV s^{-1}. The temperatures for all experiments were thermostatically controlled at 298±1 K. In order to obtain high experimental precision, each experiment was repeated three times under the same conditions.

2.3. Computational details

2.3.1 DFT calculations

Quantum-chemical based all electron calculations were performed using DFT through Dmol^3 module of Material Studio (MS) software 8.0, applying the B3LYP exchange-correlation functional [11]. Double numeric quality with polarization (DNP) basis set with the COSMO implicit solvent model (water, dielectric constant 78.54) have been used for all calculations. Besides, vibrational analysis was performed to ensure the optimized structures reaching the minimum point on potential energy surface.

2.3.2. MC Simulation

Metropolis Monte Carlo (MC) approach was utilized to explore the adsorption behavior of HMIBr on Fe(110) substrate in aqueous environment [12]. Our MC modeling was performed employing the Adsorption Locator module of MS package. Simulation annealing was carried out to search possible configurations in the space of the adsorbates on iron surface as the temperature decreased gradually. This process was repeated to identify further local energy minima.

2.3.3 MD simulation

In order to get the more accurate adsorption configurations, MD simulations of inhibitor-iron interactions were assayed using the Forcite module of MS software. The studied system consisted of a Fe(110) slab and a solvent layer (with 800 H_2O + 1 HMIBr). The built box (24.8 × 24.8 × 47.1 Å) possessed periodic boundary in order to simulate a representative part of an interface devoid of any arbitrary boundary effects. COMPASSII force field [13] was adopted, and the MD simulation was performed at 298.0 K within canonical ensemble (NVT) using a time step of 1.0 fs and a simulation time of 2000 ps. Non-bond interactions, i.e., van der Waals and electrostatic, were set as Atom-based and and Ewald summation method, respectively.

3. RESULTS AND DISCUSSION

3.1. Electrochemical impedance spectra (EIS)

The iron/solution interface characteristics in 1 M HCl solution with and without HMIBr were investigated by EIS measurement. Nyquist plots of uninhibited and inhibited acidic solutions containing different concentrations of HMIBr are given in Figure 1a, which present single depressed capacitive loops indicating that the corrosion of mild steel in researched acidic system is controlled by a charge-transfer process [14]. Figure 1b shows the values of phase angle and impedance magnitude (|Z|) increase with increasing inhibitor concentration, indicating better protection of inhibitor with higher concentrations. Moreover, only one time constant is found in the phase angle curve, which can be attributed to the relaxation effect resulting by the adsorption of corrosion inhibitor molecule [15].
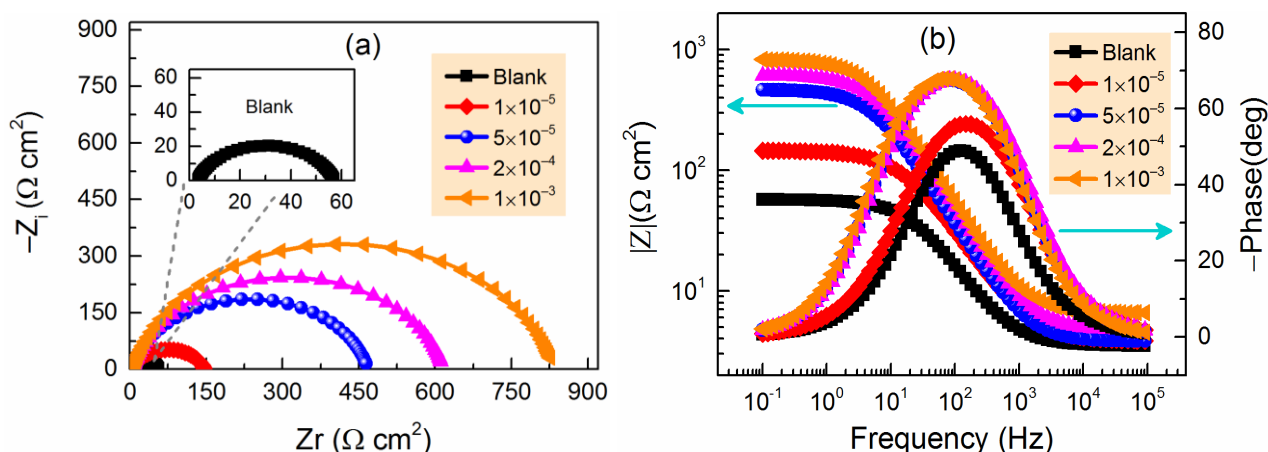
Figure 1. (a) Nyquist plots and (b) Bode plots for mild steel in 1 M HCl solution without and with different concentration of HMIBr at 298 K.

The electrochemical impedance spectra were further analyzed using the equivalent circuit. As described in Figure 2, R_s stands for the solution resistance, R_f signifies the film resistance, and R_{ct} represents the charge transfer resistance. Constant phase element (CPE) was introduced into the circuit in place of the pure capacitor of the double electric layer. The impedance of CPE can be expressed by the following formula [16, 17]:

$$Z_{CPE} = \frac{1}{Y_0(j\omega)^n} \qquad (1)$$

where Y_0 is the modulus, j is the imaginary root, ω is the angular frequency, and n represents the deviation from the ideal behavior falling between −1 and 1. When $n=0$, CPE can be regarded as a resistance, for $n=1$, a capacitance, and an inductance if $n=-1$ [18]. The capacitance of double layer (C_{dl}) values were obtained from the equation [19]:

$$C_{dl} = Y_0 \left(2\pi f_{max}\right)^{n-1} \qquad (2)$$

where f_{max} is the frequency in which the imaginary component of the impedance is maximum. The corrosion inhibition efficiency was deduced from the EIS according to the following equation:

$$IE\left(\%\right) = \frac{R_{ct} - R_{ct,0}}{R_{ct}} \times 100 \qquad (3)$$

wherein $R_{ct,0}$ and R_{ct} are the charge transfer resistance values for iron electrodes in 1 M HCl solution without and with HMIBr, respectively.
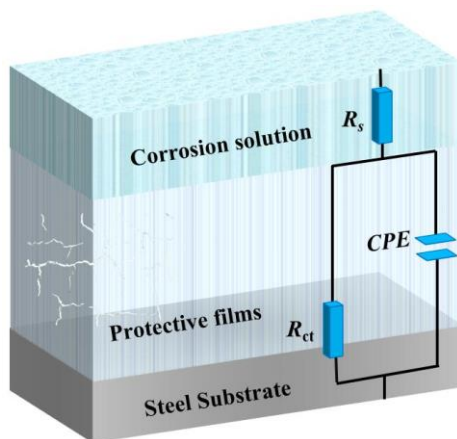

Figure 2. Equivalent circuit used to fit the EIS data.

Table 1. Impedance parameters for mild steel in 1 M HCl solution without and with diverse concentrations of HMIBr.

| C (M) | R_s (Ω cm^2) | Q | | C_{dl} (μF cm^{-2}) | R_{ct} (Ω cm^2) | ChiSq ($\times 10^{-3}$) | IE % |
		Y_0 ($\times 10^{-4}$ S s^n cm^{-2})	n				
Blank	3.472	3.148	0.823	283.1	53.65	2.62	/
1×10^{-5}	3.818	1.723	0.806	147.8	142.3	1.25	62.2
5×10^{-5}	3.807	1.097	0.838	111.5	464.4	6.38	88.4
2×10^{-4}	4.691	0.818	0.855	85.9	611.8	2.89	91.2
1×10^{-3}	6.535	0.690	0.861	72.7	827.7	3.94	93.5

As can be seen from Table 1, goodness of fit is assessed from the chisquared values, which lie in the 10^{-3} order of magnitude. The R_{ct} values increase considerably from 53.65 to 827.7 Ω cm^2 with increasing HMIBr concentration, thereby increasing the corrosion inhibition efficiency. However, the values of C_{dl} show a downward trend. The increase in R_{ct} and the decrease in C_{dl} may result from the formation of a protective barrier film at the iron/solution interface, which has caused a decrease in local dielectric constant and/or an increase in the thickness of the double layer [20].
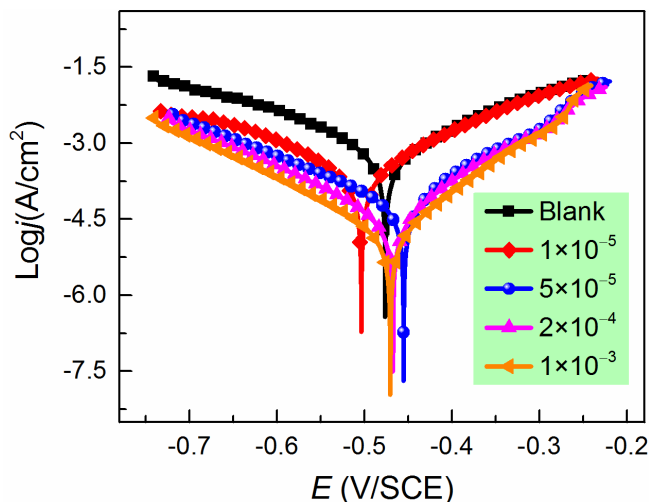
3.2. Potentiodynamic polarization method

The potentiodynamic polarization curves obtained for mild steel in 1 M HCl solution with and without HMIBr at different concentrations are HMIBr in the Figure 3. Several electrochemical corrosion descriptors, such as corrosion potentials (E_{corr}), corrosion currents densities (j_{corr}), anodic and cathodic

Tafel slopes (β_a and β_c) were obtained using Tafel extrapolation method. These parameters are summarized in Table 2. The corrosion inhibition efficiency was derived by the following formula:

$$IE\left(\%\right) = \frac{j_{corr,0} - j_{corr}}{j_{corr,0}} \times 100 \qquad (4)$$

where j_{corr} and $j_{corr,0}$ are the corrosion current densities in the presence or absence of inhibitor, respectively.

Figure 3. Potentiodynamic polarization curves of mild steel in 1 M HCl solution in the absence and presence of varying concentrations of HMIBr.

Table 2. Tafel parameters and the corresponding corrosion inhibition efficiency for the corrosion of mild steel in 1 M HCl solution in the absence and presence of different concentrations of HMIBr.

C (M)	E_{corr} (mV/SCE)	j_{corr} (μA cm^{-2})	β_a (mV dec^{-1})	$-\beta_c$ (mV dec^{-1})	IE %
Blank	−476	485.5	111	93	/
1×10^{-5}	−503	182.4	110	126	62.4
5×10^{-5}	−455	50.9	97	145	89.5
2×10^{-4}	−467	26.5	83	111	94.5
1×10^{-3}	−470	14.6	77	140	96.9

Based on the results in Figure 3 and Table 2, we can see obviously that after adding the HMIBr inhibitor, there is a decrease in both densities of anodic and cathodic current. The maximum E_{corr} displacement is −27 mV with respect to the blank, which shows that HMIBr acts as a mixed-type inhibitor, not only reducing the anodic dissolution of the mild steel but also retarding the cathodic evolution of hydrogen [21]. We also found that the inhibition efficiency increases and the corrosion current density decreases when the inhibitor concentration increases. When the concentration is 1×10^{-3} M, the inhibition reaches to the optimum value 96.9%. Moreover, the corrosion inhibition efficiencies obtained from Tafel test are basically consistent with the EIS approach. These results indicate that the adsorption of inhibitor molecules on metal substrate occupies the active sites, which can be regarded as a replacement process between the inhibitors and preadsorbed H$_2$O molecules on the iron/solution interface [22].

3.3. DFT considerations

In order to enrich the cognition on the electronic structure for our investigatived inhibitor, frontier molecular orbitals and several chemical activity descriptors were analyzed. The HOMO, LUMO as well as molecular electrostatic potential (ESP) distributions are presented in Figure 4a~4c. It is obvious that the HOMO and LUMO regions are both located on the methylimidazolium ring. This is further confirmed by the ESP map, wherein the most negative potential (red color) is around the center of aromatic ring denoting the regions of electron donation. Figure 4d displays the sigma-profiles and COSMO-cavities for HMI cation and the solvent (*i.e.*, water molecule). There are almost no overlapping peaks, indicating the hydrophobicity of long alkyl chain in cationic structure [23].
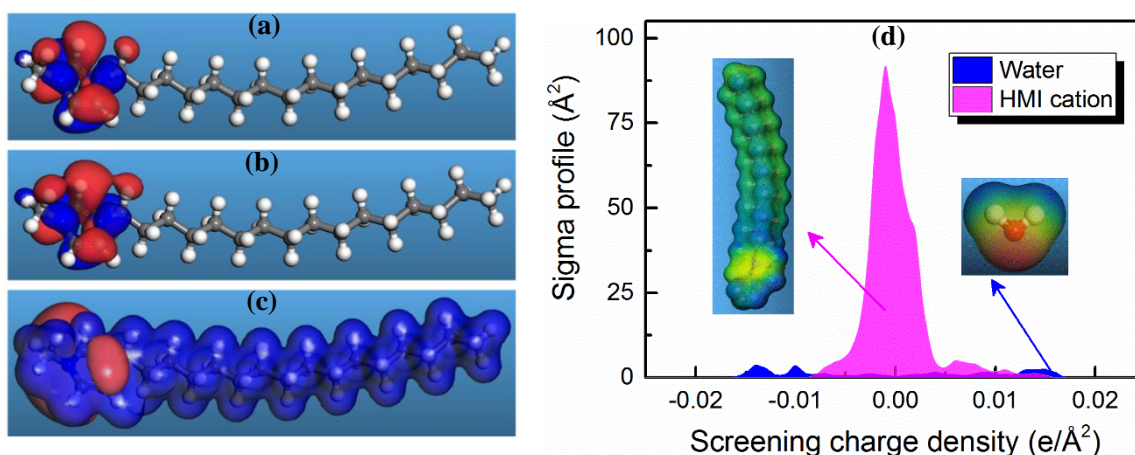
Figure 4. (a) HOMO, (b) LUMO, (c) ESP distributions, and (d) sigma-profiles & COSMO-cavities for HMI cation.

According to the Koopmans's theorem, the ionization potential (I) and electron affinity (A) can be calculated by the following relationship: $I = -E_{HOMO}$ and $A = -E_{LUMO}$. Hereon, the quantum chemical descriptors electronegativity (χ) and hardness (η) are obtained through [24, 25]:

$$\chi = (I + A)/2 = -(E_{HOMO} + E_{LUMO})/2 \qquad (5)$$

$$\eta = (I - A)/2 = (E_{LUMO} - E_{HOMO})/2 \qquad (6)$$

The fraction of electrons (ΔN) transferred between the inhibitor molecule and iron surface is calculated according to the equation [26]:

$$\Delta N = \frac{\phi_{Fe} - \chi_{inh}}{2(\eta_{Fe} + \eta_{inh})} \qquad (7)$$

where a theoretical value of work-function ϕ_{Fe}=4.82 eV used for the Fe(110) surface, η_{inh} is the electronegativity of inhibitor, while η_{Fe}=0 for bulk iron atom [27]. If $\Delta N > 0$, the corrosion inhibitor transfers its electrons to metal and vice versa if $\Delta N < 0$.

According to the results listed in Table 3, the low ΔE ($E_{LUMO}-E_{HOMO}$) value refers to the high reactivity of studied inhibitor. The positive ΔN value shows that HMIBr possesses the ability to donate electrons to mild steel surface. The dipole moment (μ) of HMI cation is 1.958 Debye (6.531×10^{-30} C·m),

which is slightly higher than that of H_2O (μ=6.18×10^{-30} C·m). The high value of dipole moment probably enhances the adsorption strength between corrosion inhibitors and metal surface [28].

Table 3. Calculated quantum chemical descriptors at the B3LYP level for HMI cation.

E_{HOMO} (eV)	E_{LUMO} (eV)	I (eV)	A (eV)	ΔE (eV)	χ (eV)	η (eV)	μ (Debye)	ΔN
−2.892	−0.185	2.892	0.185	2.707	1.538	1.353	1.958	1.212

3.4. Monte Carlo simulation
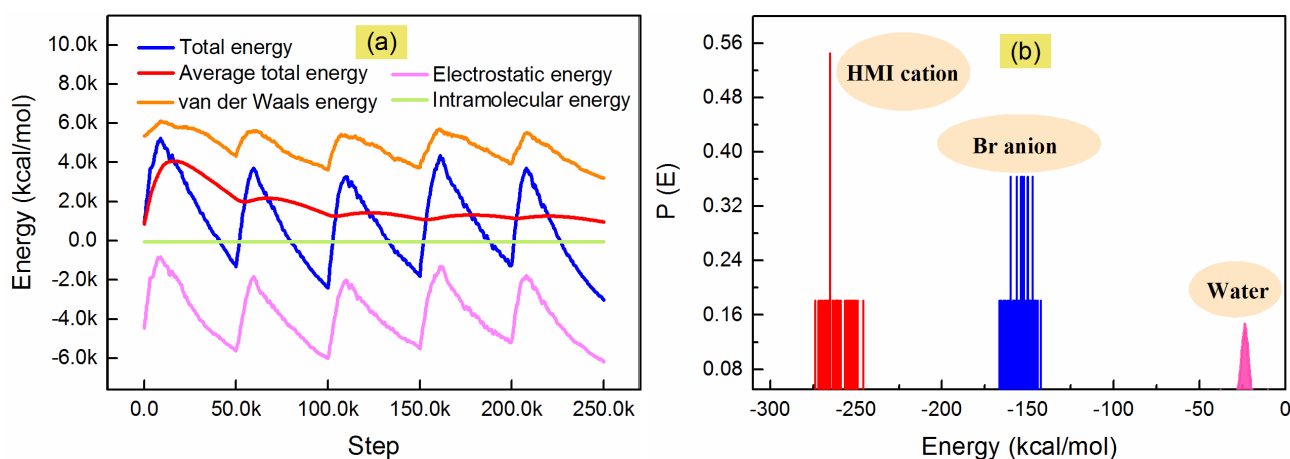
Figure 6. (a) Energy distributions as well as (b) the adsorption energy distribution of the adsorbates for HMIBr/Fe(110) system.

The MC simulation has been considered as a state-of-the-art tool to explore the adsorption behavior of individual inhibitor molecules and solvent ions on metal substrate [29]. As shown in Figure 6a, the total energy, average total energy, van der Waals energy, electrostatic energy, and intermolecular energy distributions for the Fe(110)/HMIBr/800H$_2$O system were obtained through the adsorption locator module, and the corresponding adsorption energy distributions are presented in Figure 6b. It is evident that the adsorption energies of HMI cation, Br$^-$, and H$_2$O are located at approximately −268.4, −154.5, and −23.5 kcal mol^{-1}, respectively. This confirms the validity of the hypothesis that the HMIBr inhibitor might replace water molecules.

3.5. MD simulation

MD simulation can provide more accurate information on the adsorption modes and preferred orientation of inhibitors [30]. In this account, MD simulations were carried out to investigate the adsorption of HMIBr onto the iron surface in aqueous environment. We have ensured that the simulation system reached a steady state at the end of the simulation process, in which both temperature and energy were balanced. Figure 7a gives the final adsorption configuration of HMIBr over the Fe surface. It is apparent that imidazole ring and adjacent alkyl groups adopted near-flat orientation on Fe(110) surface, while the remaining longer hydrophobic chain was placed in the corrosive medium with an inclined

structure. This adsorption mode is equivalent to forming a barrier to resist the attack of corrosion ions [31]. Besides, to quantitatively evaluate the adsorption strength, adsorption energy (E_{ads}) was introduced and calculated by the formula [32]:

$$E_{ads} = E_{total} - (E_{surf+water} + E_{inh+water}) + E_{water} \qquad (8)$$

where E_{total} gives the total energy of the whole system, E_{water} denotes the complete energy of H_2O molecules, $E_{surf+water}$ and $E_{inh+water}$ are assigned as the potential energies of the system without the inhibitor and without the iron surface, respectively. The E_{ads} in this work was gained from the average values of the optimized equilibrium configurations through a statistical method. The obtained E_{ads} value is -679.4 kJ mol^{-1}. The negative value suggests that spontaneous adsorption can be expected.
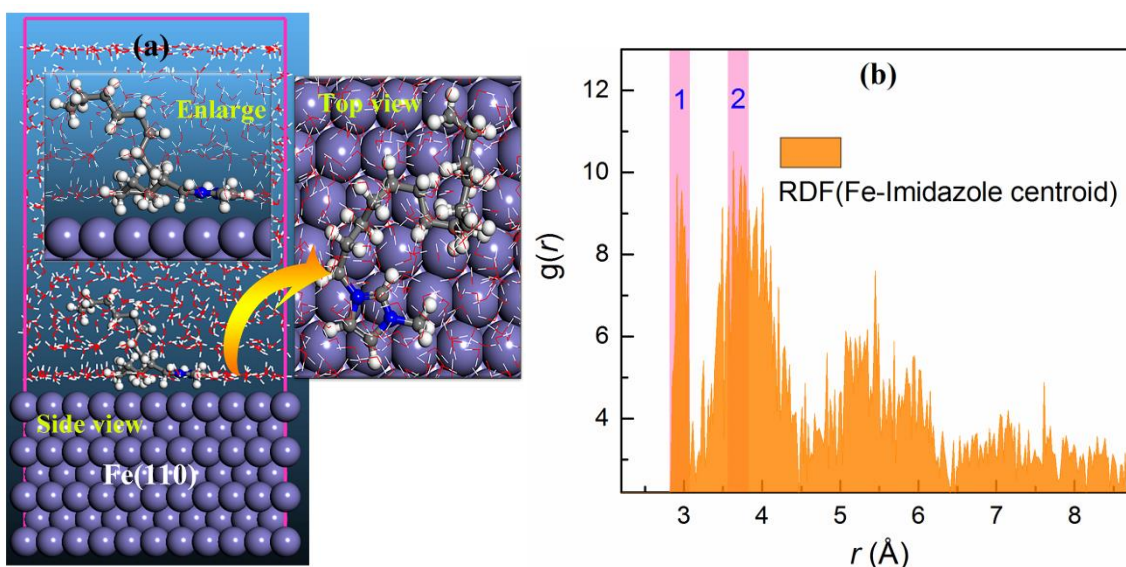

Figure 7. (a) Top and side views of the equilibrium configuration for HMIBr adsorbed on Fe(110) surface; (b) RDF curve for the centroid of imidazole ring on Fe(110) surface.

As is known, radial distribution function (RDF), $g(r)$, is a very useful tool to estimate the distance between the inhibitor and metal surface. Generally, a small distance (<3.5Å) indicates that the interaction mode is a chemisorption type, while a distance greater than 3.5 Å is associated to physisorption [33, 34]. In our case, the RDF curve of imidazole centroid and Fe atoms was analyzed. As shown in Figure 7b, the first peak is located near 3 Å, which can be attributed to the chemical bonds formed between the imidazole ring and iron atoms. Moreover, several other peaks that located outside 3.5 Å may be derived from physical interactions by bromide ions and alkyl chains.

3.6. Analysis of anti-corrosion mechanism

In order to present the inhibition mechanism more intuitively, an adsorption model was proposed and given in Figure 8. It's not hard to understand the iron substrate would be eroded by corrosive ions such as H_3O^+ and Cl^- in the blank HCl medium. This is the so-called pitting phenomenon. In particular, in the uninhibited HCl solution, the anodic reaction of iron is the dissolution of metallic iron (Fe^0) to

ferrous cations (Fe^{2+}) [35]. Thus bromine ions will quickly adsorb on the protonated mild steel surface when adding the HMIBr inhibitor, which can be considered as a bridge joining the HMI cations and the positively charged iron surface. Consequently, a self-assembled protective layer was formed, which effectively isolates the iron from contacting with corrosive media. We also consider that the hybridization interaction between the inhibitor molecules and the 3d-orbitals of the surface iron atoms plays a key role in the adsorption behavior.
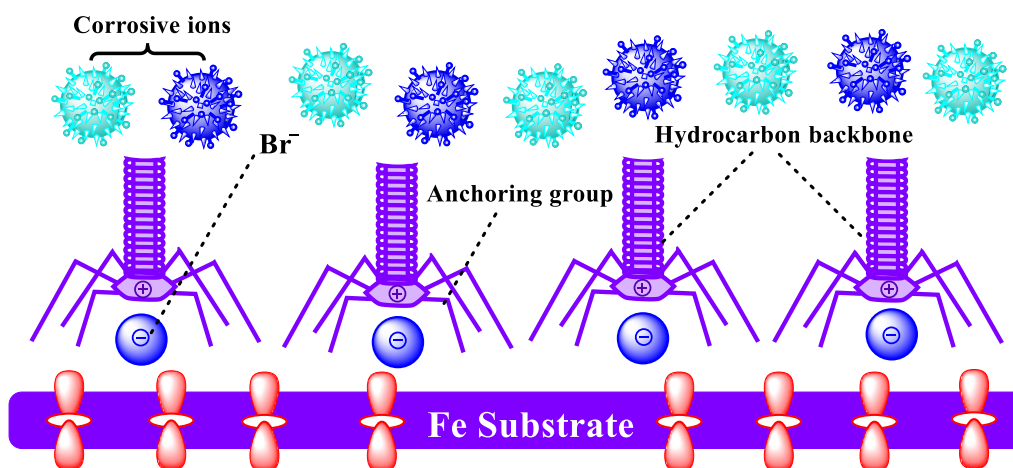
Figure 8. Schematic representation for the inhibition mechanism of HMIBr on iron surface.

4. CONCLUSIONS

In summary, the present work aimed to assess the efficiency of an ionic liquid on the corrosion of mild steel in 1 M HCl solution. Overall, the mutually supported experimental and theoretical findings show that HMIBr is an excellent candidate for the use as corrosion inhibitor for mild steel. The inhibition performance increases with the increase of selected inhibitor concentration. Impedance results shows that the addition of tested inhibitor to HCl solution increasing the polarization resistance but decreasing the capacitance. Potentiodynamic polarization curves have revealed that the HMIBr act as a mixed-type inhibitor. HMIBr was found to suppress the corrosion through spontaneous chemical and physical adsorption on the iron surface. DFT calculations, MC/MD simulations, and RDF analysis for the investigated inhibitor have further clarified the anti-corrosion mechanism. All the insights gained from this work could be helpful to encourage researchers to develop more ionic liquid-based corrosion inhibitors for metallic materials.

References

1. B. Hou, X. Li, X. Ma, C. Du, D. Zhang, M. Zheng, W. Xu, D. Lu and F. Ma, *npj Materials*

Degradation, 1 (2017) 4.

2. L. T. Popoola, *Corros. Rev.*, 37 (2019) 71-102.
3. A. Singha and M. A. Quraishi, *J. Mater. Environ. Sci.*, 6 (2015) 224-235.
4. D. Kesavan, M. Gopiraman and N. Sulochana, *Chem. Sci. Rev. Lett*, 1 (2012) 1-8.
5. L. Guo, I. B. Obot, X. Zheng, X. Shen, Y. Qiang, S. Kaya and C. Kaya, *Appl. Surf. Sci.*, 406 (2017) 301-306.
6. M. Christov and A. Popova, *Corros. Sci.*, 46 (2004) 1613-1620.
7. C. K. Skylaris, *Science*, 351 (2016) 1394-1395.
8. Y. Qiang, S. Zhang, L. Guo, X. Zheng, B. Xiang and S. Chen, *Corros. Sci.*, 119 (2017) 68-78.
9. C. Verma, E. E. Ebenso and M. A. Quraishi, *J. Mol. Liq.*, 233 (2017) 403-414.
10. A. Yousefi, S. Javadian, N. Dalir, J. Kakemam and J. Akbari, *RSC Adv.*, 5 (2015) 11697-11713.
11. M. P. Andersson and P. Uvdal, *J. Phys. Chem. A*, 109 (2005) 2937-2941.
12. I. B. Obot, A. Madhankumar, S. A. Umoren and Z. M. Gasem, *J. Adhes. Sci. Technol.*, 29 (2015) 2130-2152.
13. H. Sun, *J. Phys. Chem. B*, 102 (1998) 7338-7364.
14. X. G. Zhang, X. Liu, W. P. Dong, E. D. Fan, Z. H. Bai, G. K. Hu, P. Yi, K. Xiao and Y. H. Huang, *Int. J. Electrochem. Sci.*, 14 (2019) 2683-2692.
15. S. Xu, S. Zhang, L. Guo, L. Feng and B. Tan, *Materials*, 12 (2019) 1339.
16. G. J. Brug, A. L. G. Vandeneeden, M. Sluytersrehbach and J. H. Sluyters, *J. Electroanal. Chem.*, 176 (1984) 275-295.
17. A. Popova, S. Raicheva, E. Sokolova and M. Christov, *Langmuir*, 12 (1996) 2083-2089.
18. S. Shen, X. Y. Guo, P. Song, Y. C. Pan, H. Q. Wang, Y. Wen and H. F. Yang, *Appl. Surf. Sci.*, 276 (2013) 167-173.
19. T. M. Lv, S. H. Zhu, L. Guo and S. T. Zhang, *Res. Chem. Intermed.*, 41 (2015) 7073-7093.
20. 2M. I. Awad, *J. Appl. Electrochem.*, 36 (2006) 1163-1168.
21. Sudheer and M. A. Quraishi, *Arab. J. Sci. Eng.*, 38 (2013) 99-109.
22. M. A. Deyab, *Desalination*, 439 (2018) 73-79.
23. L. del Olmo, R. López and J. M. García de la Vega, *Int. J. Quantum Chem.*, 113 (2013) 852-858.
24. P. Geerlings, F. De Proft and W. Langenaeker, *Chem. Rev.*, 103 (2003) 1793-1873.
25. N. Khalil, *Electrochim. Acta*, 48 (2003) 2635-2640.
26. I. B. Obot, D. D. Macdonald and Z. M. Gasem, *Corros. Sci.*, 99 (2015) 1-30.
27. L. Guo, S. Zhu, S. Zhang, Q. He and W. Li, *Corros. Sci.*, 87 (2014) 366-375.
28. W. Gong, B. Xu, X. Yin, Y. Liu, Y. Chen and W. Yang, *J. Taiwan Inst. Chem. Eng.*, 97 (2019) 466-479.
29. A. H. Juffer, P. Argos and J. DeVlieg, *J. Comput. Chem.*, 17 (1996) 1783-1803.
30. S. Kato and H. X. Hu, *Surf. Sci.*, 357 (1996) 891-895.
31. O. Dagdag, A. El Harfi, O. Cherkaoui, Z. Safi, N. Wazzan, L. Guo, E. D. Akpan, C. Verma, E. E. Ebenso and R. T. T. Jalgham, *RSC Adv.*, 9 (2019) 4454-4462.
32. L. H. Madkour, S. Kaya and I. B. Obot, *J. Mol. Liq.*, 260 (2018) 351-374.
33. J. P. Zeng, J. Y. Zhang and X. D. Gong, *Comput. Theor. Chem.*, 963 (2011) 110-114.
34. L. Guo, X. Ren, Y. Zhou, S. Xu, Y. Gong and S. Zhang, *Arab. J. Chem.*, 10 (2017) 121-130.
35. Z. Zhang, N. C. Tian, X. D. Huang, W. Shang and L. Wu, *RSC Adv.*, 6 (2016) 22250-22268.